Effect of Gelatin Concentration on Methylene Blue Transport in Three-Dimensional Gelatin Matrices

Joshua Lee[1]

Received July 6, 2026
Accepted October 22, 2026
Electronic access November 30, 2026

The extracellular matrix (ECM) plays an important role in regulating molecular transport within biological tissues, including the distribution of therapeutic molecules in tumor microenvironments. However, it is difficult to distinguish individual factors that influence transport behavior due to the complexity of the native ECM. To examine the effect of the gelatin concentration on the transport of methylene blue, a model small molecule, gelatin matrices were used as a simplified three-dimensional ECM model. Gelatin matrices with concentrations of 1%, 2%, 5% and 10% (w/v) were prepared, and the transport of methylene blue was evaluated by both a top-view measurement of the dye spreading on the surface and a side-view measurement of dye penetration. Three independent gelatin matrices were analyzed for each concentration (n = 3). Over the 60 min experimental period, methylene blue transport decreased with increasing gelatin concentration. In the surface spreading experiment, the relative increase in spread radius at 60 min was approximately 50% for the 1% gelatin matrices, compared to approximately 10% for the 10% matrices. Although oscillatory rheometry showed that different gelatin concentrations impacted the viscoelastic properties of the matrices, structural properties related to molecular transportation – such as pore size, porosity, tortuosity, and permeability – were not directly measured. The results indicate that there is a relationship between the amount of gelatin used and the amount of methylene blue transported but do not identify one specific mechanism to account for the difference in results. This simplified experimental system, in addition to providing an accessible approach for visualizing concentration-dependent transport in three-dimensional matrices, may also serve as a foundation for future studies incorporating hydrated-state structural characterization and quantitative transport modeling.

Keywords: Gelatin Matrices; Methylene Blue; Gelatin Concentration; Dye Transport; Penetration

Introduction

The extracellular matrix (ECM) is a three-dimensional network of proteins, polysaccharides, and other macromolecules that provides structural support to cells and contributes to the regulation of cellular behavior. In tumors, changes in ECM composition and organization can change the local microenvironment and influence the transport of therapeutic and diagnostic molecules through tissue [1–4]. Therefore, understanding how the properties of a three-dimensional matrix affect molecular transport is important for studying drug penetration and distribution within complex biological environments.

Molecular transport through the ECM is influenced by multiple interacting factors such as, polymer content, matrix organization, molecular interactions, and the physicochemical properties of the molecule itself [5–7]. Because ECM composition and structure differ significantly among tissue types and disease states, these factors are difficult to separate in native tissues. In order to address this complexity, simplified three-dimensional matrix systems can be used to study specific factors under controlled conditions [6,7]. These models are not meant to replicate all the characteristics of a native ECM. Instead, these models allow researchers to focus on selected factors that may influence molecular transport.

Gelatin is a collagen-derived biopolymer that is widely used in three-dimensional biomaterial and tissue-modeling applications because of its biocompatibility, accessibility, and ease to prepare at different concentrations [8–10]. Changing gelatin concentration provides a simple way to control how much polymer is present in a hydrated three-dimensional matrix. However, gelatin concentration itself cannot be used to directly determine specific properties such as stiffness, porosity, pore size, or tortuosity, as these properties would require separate measurements [11–13]. Therefore, gelatin concentration can instead be treated as an experimentally controlled formulation parameter for investigating concentration-dependent changes in molecular transport.

Methylene blue has several useful properties making it well suited to this application. It is a small, water-soluble, intensely colored molecule. Its color allows us to track its motion through a transparent/translucent matrix with the naked

[1] *Bellevue High School, Washington, USA*

© The National High School Journal of Science 2026

eye [14,15]. These properties make methylene blue useful for examining transport in a simple, three-dimensional matrix system. Observing the extent of diffusion of dye as a function of time provides an easily understood demonstration of transport differences between matrices of various polymer concentrations.

In this study, gelatin matrices of different concentrations, specifically 1%, 2%, 5% and 10%, have been prepared as simplified ECM models to observe how methylene blue molecule travels through different concentrations of gelatin. The transport rates of the methylene blue were monitored over time and were compared between different gelatin concentrations. Rather than assuming that gelatin concentration directly represents a particular mechanical or structural property of the ECM, we treated gelatin concentration as the experimentally controlled variable. Additionally, methylene blue transport was treated as the measured outcome. As shown in Scheme 1, our goal is to create a simple experimental system that can be used to visualize the effect of polymer concentration on molecular transport behavior in a three-dimensional matrix. To provide a quantitative basis for this relationship, storage modulus (G') and loss modulus (G'') were measured by oscillatory rheometry for all gelatin concentrations. We hypothesized that the methylene blue surface spreading and penetration would be progressively reduced over time as gelatin concentration increased.

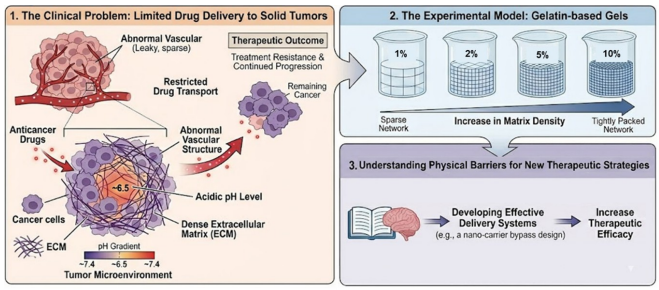

Scheme 1. Schematic overview of the study: Mimicking the extracellular matrix in the tumor microenvironment (TME) and its impact on drug delivery systems.

Methods

Preparation of Gelatin Matrix

Gelatin matrices were prepared using Type B bovine gelatin (TUOTAI, product no. 728047095390; Amazon ASIN: B09QZW3JMJ), purchased through Amazon. The Bloom strength was not provided in the supplier's product specifications available to the authors. Gelatin solutions were prepared at concentrations of 1%, 2%, 5%, and 10% (w/v) in distilled water. The gelatin powder was hydrated in distilled water for 10 min at room temperature and then heated in a water bath at 50–60 °C until it completely dissolved and became transparent. The resulting solutions were poured into cylindrical cups (4.00 cm in diameter and 4.00 cm in height), with 13 mL of gelatin solution added to each cup. The gelatin solutions made from this process had gel thickness that was measured to be approximately 2 cm. These samples were then refrigerated at 4 °C for 1 h to allow gelation. Before the transport experiments, the samples were removed from refrigeration and equilibrated at 25 °C for 10 min. All transport experiments were later conducted at 25 °C, and the gelatin matrices maintained their gel form throughout the 60-min experimental period. The same sample preparation volume and dimensions were kept throughout all gelatin concentrations in order to ensure that the experiments were consistent.

Dye Transport Experiment Setup

Methylene blue (laboratory grade, 1% w/v aqueous solution; Supplier: ALDON Corporation) was used as a model small-molecule compound in order to examine dye transport through the gelatin matrices. Two complementary experimental approaches were used for this experiment.

- Surface Dye Spread Method (Droplet Method)

  A fixed volume of 50 μL of methylene blue solution was pipetted onto the center of each gelatin sample, and the spread of methylene blue on the gelatin surface was monitored with top-view imaging at predetermined time intervals (0, 5, 10, 20, 30, and 60 minutes).

- Dye Penetration Depth Method (Overlay Method)

  Methylene blue solution was applied to the top of each gelatin matrix using a 1-mL syringe. A single drop was applied, and it was allowed to spread across the gel surface and cover the surface before penetration measurements were taken. The penetration of the visible dye front into the gelatin matrix was monitored by side-view imaging at the same predetermined time intervals (0, 5, 10, 20, 30, and 60 min).

Image acquisition and Quantification

Images were taken at predetermined time intervals (0, 5, 10, 20, 30, and 60 min) using a smartphone camera under the same lighting conditions. The camera was kept at the same distance and position from the samples for all images taken. The 0-min image was taken immediately after when methylene blue was applied onto the sample. For the droplet method, surface spreading was quantified as the relative increase in surface spread radius compared with the initial radius using the following equation:

where represents the surface spread radius at time , and represents the initial surface spread radius measured at 0 min.

© The National High School Journal of Science 2026

For the overlay method, penetration was quantified as the relative increase in penetration depth compared with the initial penetration depth using the following equation:

where represents the penetration depth measured at time , and represents the initial penetration depth measured at 0 min.

All measurements were analyzed using image analysis software (ImageJ) to ensure that the measurements were taken consistently. The visible boundary of the methylene blue-stained region was manually traced instead of being identified using automated thresholding or segmentation. For the surface spreading experiment, the distance from the center of the applied dye to the outer edge of the visible stained region that was manually identified was measured as the surface spread radius. The distance from the gelatin surface to the deepest clearly visible dye front was manually identified and measured as the penetration depth when conducting the penetration experiment. The same criteria for identifying the dye boundary were used across all gelatin concentrations, replicates, and time points.

Rheological Characterization

Dynamic oscillatory rheometry was performed using a HAAKE MARS iQ Air rheometer (Thermo Fisher Scientific) with a parallel plate geometry (40 mm diameter, 0.5 mm gap). Gelatin samples (1, 2, 5, and 10% w/v) were loaded onto the lower plate and equilibrated at 25 °C for 5 minutes. An amplitude sweep (0.1–10% strain at 1 Hz) was first conducted to determine the linear viscoelastic region (LVR) for each concentration. The strain amplitude corresponding to the LVR was then fixed at 0.1% for all subsequent frequency sweep measurements. Frequency sweeps were conducted from 10 to 0.1 Hz at 25 °C using logarithmic ramp mode with 13 points per decade. Storage modulus (G') and loss modulus (G'') were recorded as functions of frequency. Three independent measurements were performed for each gelatin concentration ($n = 3$), and the mean G' values were used for comparing the elastic response across the different concentrations.

Sample preparation for Scanning electron microscope (SEM)

Gelatin samples prepared at different concentrations (1%, 2%, 5%, and 10% w/v in distilled water) were freeze-dried for 48 h. The dried samples were sputter-coated with platinum (Pt) for 60 s and observed using a scanning electron microscope (SNE-3200M, SEC/ETS, Korea). SEM images were acquired at a magnification of 100×.

Results

Surface Dye Spread Behavior in Gelatin Matrices

The Droplet Method was used to measure the surface spread behavior of methylene blue dye on the gelatin matrices with a concentration of 1%, 2%, 5%, and 10% (w/v), respectively. The experiment was conducted by pipetting a 50 μL methylene blue solution droplet on the center of the gelatin sample. The spreading of the surface dye was observed in the 0, 5, 10, 20, 30, and 60-min time intervals from the top view imaging. Figure 1 presents representative time-lapse images for all concentrations studied, with three independent gelatin matrices analyzed for each concentration ($n = 3$).

The 1% gelatin matrices exhibited the greatest increase in surface dye spread over the 60-min experimental period, followed by the 2%, 5%, and 10% gelatin matrices. At 60 min, the relative increase in surface spread radius was $48.17 \pm 3.42\%$, $29.57 \pm 8.01\%$, $13.81 \pm 3.00\%$, and $9.88 \pm 8.11\%$ for the 1%, 2%, 5%, and 10% gelatin matrices, respectively.

Clearly, as shown in Figure 2, the surface dye spreading behavior in gelatin matrices was significantly affected by the concentration of the gelatin matrices as the gelatin matrices with higher concentrations showed a decrease in surface dye spread. Moreover, the difference between gelatin matrix samples with different concentrations became more significant in the later time intervals. These observations were consistently shown in all three gelatin matrices of each concentration. These results show that gelatin concentrations have direct effect on the methylene blue spreading on the matrix surface under the given conditions used in this study. However, it was not possible to draw conclusions regarding transport mechanisms on the basis of spreading by using this experiment alone. More information regarding transport mechanisms will be presented and further considered in the Discussion section later on.

Dye Penetration Depth in Gelatin Matrices

The dye penetration depths were evaluated for the 2%, 5%, and 10% (w/v) gelatin matrices using the Overlay Method. The matrices made from the 1% solution did not show a consistently and reproducibly well-defined visible penetration depth and thus were excluded from the depth analysis. For the other concentrations, a 1-mL syringe was used to place one drop of methylene blue solution onto the top of the gelatin matrix, and the drop was allowed to sit and spread on the top surface of the gelatin matrix. We assessed the penetration of the visible dye front by taking side-view images of the gelatin matrix at 0, 5, 10, 20, 30, and 60 min. Figure 3 shows representative time-lapse images for the examined gelatin concentrations. The images shown are for three separate gelatin matrices for each concentration ($n = 3$).

© The National High School Journal of Science 2026

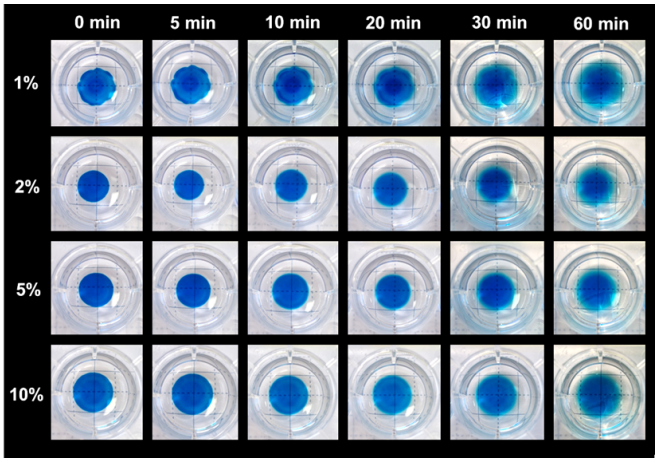

Figure. 1 Time-dependent surface spreading of methylene blue on gelatin matrices with different gelatin concentrations. Representative top-view images of methylene blue applied to 1%, 2%, 5% and 10% (w/v) gelatin matrices at 0, 5, 10, 20, 30, and 60 min. An identical volume of methylene blue solution was applied to the surface of each gelatin matrix, and the surface spread radius was measured at each time point.

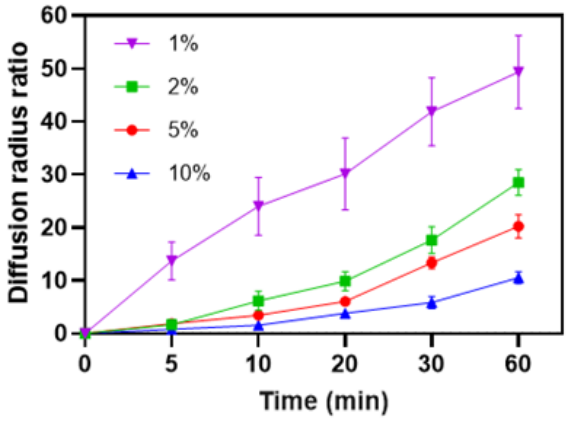

Figure. 2 Time-dependent relative increase in surface spread radius of methylene blue on gelatin matrices with different gelatin concentrations. The relative increase in surface spread radius was determined for 1%, 2%, 5%, and 10% (w/v) gelatin matrices at 0, 5, 10, 20, 30, and 60 min. Values were calculated relative to the initial surface spread radius at 0 min and are presented as mean $\pm$ SD ($n = 3$ independent gelatin matrices per concentration).

Methylene blue penetration increased over time in the 2%, 5%, and 10% gelatin matrices. At the early time points, the differences among the three concentration groups were relatively small. As the experimental period progressed, the penetration profiles became increasingly separated according to gelatin concentration. At 60 min, the relative increase in penetration depth was $72.65 \pm 12.04\%$, $64.55 \pm 7.35\%$, and $45.60 \pm 8.35\%$ for the 2%, 5%, and 10% gelatin matrices, respectively. Thus, the 2% gelatin matrices exhibited the greatest increase in penetration depth, the 5% matrices showed an intermediate increase, and the 10% matrices exhibited the smallest increase at the end of the experimental period.

As shown in Figure 4, the extent of penetration was consistently concentration-dependent at the later time points, as the relative increases in penetration depth were larger for lower gelatin matrix concentrations compared with higher concentrations at the later time points. This trend was evident in the three replicates conducted at each concentration. Combined with the surface spreading experiments, these findings indicate that there is a correlation between gelatin concentration and methylene blue transport within the gelatin gels. However, while the penetration depth assays yield significant information regarding dye transport as a function of gelatin matrix concentration, they alone cannot determine the physical or physicochemical mechanism underlying the concentration-dependent differences.

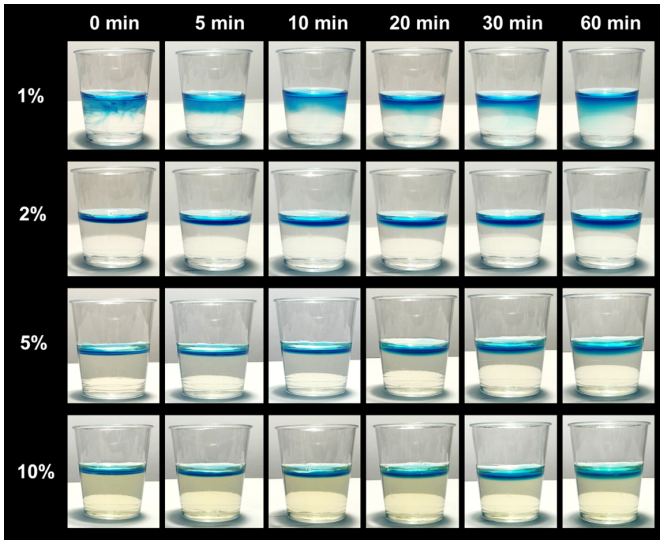

Figure. 3 Time-dependent penetration of methylene blue into gelatin matrices with different gelatin concentrations. Representative side-view images of methylene blue penetration in 1%, 2%, 5%, and 10% (w/v) gelatin matrices at 0, 5, 10, 20, 30, and 60 min. For the Overlay Method, a single drop of methylene blue solution was applied to the top of each gelatin matrix using a 1-mL syringe and allowed to spread across the gel surface. Penetration depth was determined from the gel surface to the deepest clearly visible dye front at each time point. The 1% gelatin matrices are shown for qualitative purposes only and were excluded from depth of penetration analyses due to the inability to determine a consistent delineation of methylene blue penetration.

Below in Table 1 are the summarized quantitative results

© The National High School Journal of Science 2026

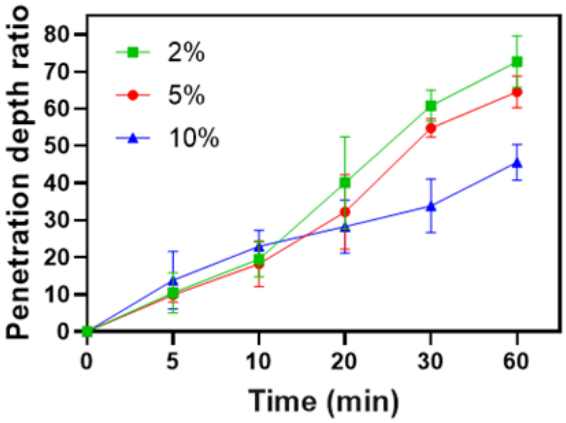

Figure. 4 Time-dependent relative increase in penetration depth of methylene blue in gelatin matrices with different gelatin concentrations. The relative increase in penetration depth was determined for 2%, 5%, and 10% (w/v) gelatin matrices at 0, 5, 10, 20, 30, and 60 min. Values were calculated relative to the initial penetration depth measured at 0 min and are presented as mean ± SD ($n = 3$ independent gelatin matrices per concentration). The 1% gelatin matrices were excluded from quantitative analysis because a reproducible penetration front could not be reliably defined.

of the surface spreading experiments and the penetration experiments across all the measured time points and the gelatin concentrations.

Data are presented as mean ± SD ($n = 3$ independent gelatin matrices per concentration). Relative increases were calculated with respect to the initial value measured at 0 min. The 1% gelatin matrices were excluded from quantitative penetration-depth analysis because a reproducible visible penetration front could not be reliably defined.

Viscoelastic Characterization via Oscillatory Rheometry

The viscoelastic properties of gelatin matrices were characterized by oscillatory rheometry to independently assess concentration-dependent differences in their mechanical properties. Amplitude sweep measurements were performed at 1 Hz over an oscillatory strain range of 0.1–10%. The corresponding storage modulus, (G'), shown in Figure 5A, revealed a large concentration-dependent variation across the tested range of strains. The descending ranking of the gelatin matrices by G' values were 10%, 5%, 2%, and 1% matrices. In general, the G' values tended to decrease with increasing strain; this was most obvious for the 2%, 5%, and 10% gelatin matrices. The loss modulus (G'') was also dependent on the gelatin concentration but had values that were generally lower (compared to those of G') especially for higher gelatin concentrations. The 10% gelatin matrices demonstrated the highest G'' values for most of the strain range followed by the 5%, whereas the G'' values of the 1% and 2% gelatin matrices were significantly lower compared to those of the other two samples. Altogether, these results show concentration-dependent differences in both the elastic components and viscous components of the gelatin matrices.

Frequency sweep measurements were then conducted at 0.1% strain over a frequency range of 0.1–10 Hz at 25°C. As shown in Figure 5B, G' showed a strong dependence on gelatin concentration across the measured frequency range. The 10% gelatin matrices had the largest G' values, approximately 800 to 1,000 Pa over most of the measured frequency range, followed by the 5% matrices with G' values of approximately 300 to 500 Pa. On the other hand, much smaller G' values were seen for the 2% and 1% gelatin matrices, typically under approximately 25 Pa and 10 Pa, respectively. The corresponding G'' values were lower than those of G' for most of the frequency ranges but were much more frequency dependent. Higher concentration gelatin matrices, particularly the 10% and 5% gelatin groups, had higher G'' values compared to lower concentration matrices.

The storage modulus of the gelatin matrices was still highly dependent on the gelatin concentration with the hierarchy 10% > 5% > 2% > 1%, although a slight variation of the order was observed at higher frequencies. Furthermore, storage modulus of the matrices (G') was higher compared to the loss modulus (G'') for most testing conditions, which indicates that the gelatin matrices responded primarily elastically under the conditions of these oscillatory measurements. Overall, oscillatory rheometry revealed a concentration-dependent increase in the elastic response of the gelatin matrices. Note that these oscillatory rheometry data were obtained to better characterize the concentration-dependent differences in matrix mechanics. They do not directly represent the hydrated pore size, porosity, tortuosity, or permeability.

Microstructural Characterization via SEM

Scanning electron microscopy (SEM) was carried out to investigate if there was a correlation between the dye transport behavior observed and the underlying microstructure features. Figure 6 displays the SEM images of freeze-dried gelatin at 100× magnification for each concentration (1%, 2%, 5% and 10%).

The freeze-dried samples exhibited concentration-dependent differences in morphology. While the 1% sample appears to be mainly lamellar or layered in structure, the remaining samples are visually distinct with differences in the apparent size and void space organization. However, pore size and porosity were not quantitatively measured in the present study.

It is important to note that the SEM images represent the

© The National High School Journal of Science 2026

Table 1 Quantitative summary of methylene blue surface spreading and penetration in gelatin matrices

Measurement	Time (min)	1%	2%	5%	10%
Relative increase in surface spread radius (%)	0	0.00 ± 0.00	0.00 ± 0.00	0.00 ± 0.00	0.00 ± 0.00
	5	13.21 ± 7.34	2.15 ± 2.74	2.62 ± 1.16	3.05 ± 2.88
	10	19.31 ± 9.02	5.11 ± 2.50	4.50 ± 1.43	3.04 ± 2.08
	20	29.39 ± 13.13	7.02 ± 1.96	6.65 ± 2.66	4.96 ± 3.23
	30	42.24 ± 5.82	19.92 ± 10.50	9.72 ± 2.82	7.44 ± 2.66
	60	48.17 ± 3.42	29.57 ± 8.01	13.81 ± 3.00	9.88 ± 8.11
Relative increase in penetration depth (%)	0	-	0.00 ± 0.00	0.00 ± 0.00	0.00 ± 0.00
	5	-	10.46 ± 9.38	9.87 ± 3.33	13.79 ± 13.45
	10	-	19.48 ± 8.23	18.21 ± 10.50	22.92 ± 7.57
	20	-	40.08 ± 21.42	32.24 ± 17.50	28.24 ± 12.38
	30	-	60.78 ± 7.39	54.74 ± 4.38	33.82 ± 12.39
	60	-	72.65 ± 12.04	64.55 ± 7.35	45.60 ± 8.35

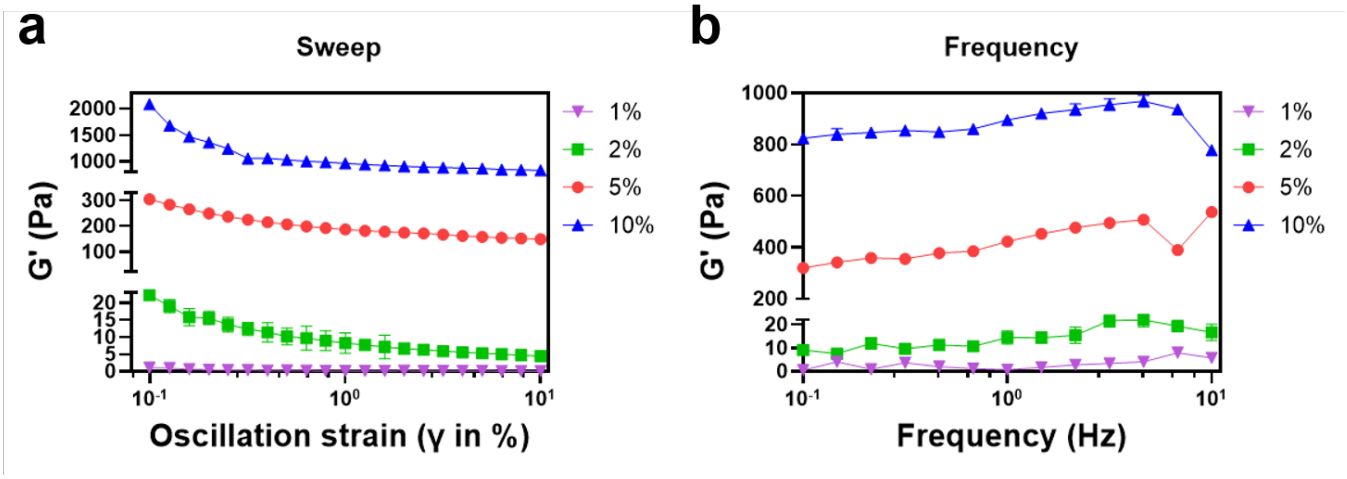

Figure. 5 Viscoelastic characterization of gelatin matrices by oscillatory rheometry. (A) Storage modulus (G'; filled symbols) and loss modulus (G''; open symbols) as functions of oscillatory strain (0.1–10%) measured at 1 Hz for 1%, 2%, 5%, and 10% (w/v) gelatin matrices. (B) G' and G'' as functions of frequency (0.1–10 Hz) measured at 0.1% strain and 25 °C. G' showed a pronounced concentration-dependent increase, with the overall modulus ranking maintained as $10\% > 5\% > 2\% > 1\%$. Throughout the experiment, G'' was generally lower than G' and also showed greater frequency-dependent variation. Data are presented as mean ± SD ($n = 3$ independent samples).

morphology of freeze-dried samples rather than the structure of the gelatin matrices in their hydrated state during the dye transport experiments. Freezing and subsequent sublimation of water in the hydrogel can change the structure and morphology and can introduce structural features into the network not representative of the hydrated network. Therefore, the SEM observations were interpreted only as qualitative differences in dried-state morphology and were not used to determine hydrated pore size, porosity, interconnectivity, tortuosity, or permeability.

Although the concentration-dependent differences in dried morphology were observed alongside differences in methylene blue transport behavior, this SEM analysis does not establish a causal relationship between these observations. More information is required including the direct characterization of the hydrated matrix in order to determine if the observed

© The National High School Journal of Science 2026

differences in methylene blue transport through hydrogels of various gelatin concentrations are due to the pore structure of the hydrated gels.

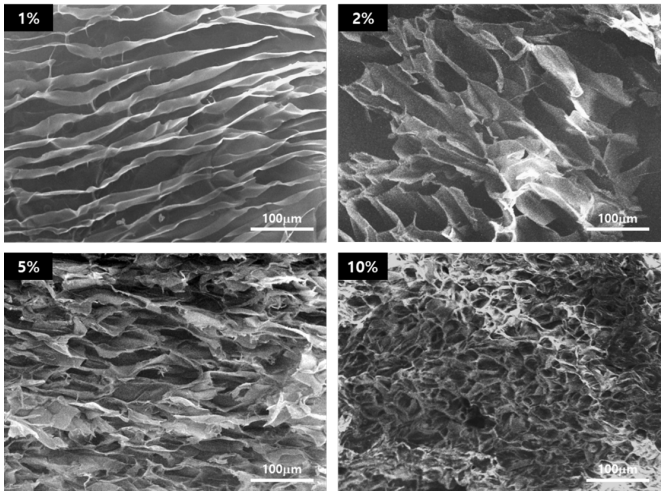

Figure. 6 Scanning electron microscopy (SEM) images showing the qualitative dried-state morphology of freeze-dried gelatin samples prepared at different concentrations (1%, 2%, 5%, and 10% (w/v) in distilled water). All images were acquired using an SNE-3200M (ETS, Korea) at a magnification of 100×. The scale bar represents 100 μm. SEM images were interpreted as qualitative dried-state morphology and not as measurements of hydrated pore structure.

Discussion

Overall, this study investigated the relationship between the gelatin concentration and the methylene blue transport in three-dimensional matrices. The overall methylene blue transport behavior, including surface spreading and penetration behaviors, was found to be concentration dependent. At 60 min, the relative increase in surface spread radius was $48.17 \pm 3.42\%$, $29.57 \pm 8.01\%$, $13.81 \pm 3.00\%$, and $9.88 \pm 8.11\%$ for the 1%, 2%, 5%, and 10% gelatin matrices, respectively. Similarly, the relative increase in penetration depth at 60 min was $72.65 \pm 12.04\%$, $64.55 \pm 7.35\%$, and $45.60 \pm 8.35\%$ for the 2%, 5%, and 10% matrices, respectively. These findings are broadly consistent with previous studies showing that molecular transport in hydrogel or ECM-like matrices can vary with matrix composition and material properties[5,13,16].

Moreover, qualitative information about the structure of the gelatin matrix was also provided by SEM imaging of the gelatin samples. However, it must be emphasized that freezing and removing water may induce structural changes, which might have a significant impact on the structure of hydrogel materials[17]. Therefore, although different structures were observed for samples with different gelatin concentrations, with a lamellar structure for the 1% sample and porous structures for samples with higher concentrations, they should not be considered direct evidence of the structure of the pore network in the hydrated gelatin gels during transport experiments, and conclusions about pore size, porosity, pore interconnectivity, tortuosity and permeability as a function of the gelatin concentration can neither be drawn nor quantified using these images.

The observed differences in dried-state morphology occurred alongside the concentration-dependent differences in methylene blue spreading and penetration. However, this correspondence does not establish that the morphological features observed by SEM caused the differences in dye transport. The observed transport behavior may have resulted from a variety of other concentration-dependent changes in the matrix, including its mechanical properties, the dye-matrix interaction, wetting, capillary transport and other physicochemical processes. Further work is required, including controlled transport studies and characterization of the structures in the hydrated state in order to identify the particular mechanisms that may be responsible for observed differences. Rheological characterization also revealed concentration-dependent differences in the viscoelastic properties of the gelatin matrices. For most of the conditions studied, the storage modulus (G') was greater than the loss modulus (G''), and G' tended to increase with increasing gelatin concentration, with the overall ranking of $10\% > 5\% > 2\% > 1\%$. Previous studies have also reported similar concentration and formulation-dependent changes in the mechanical and viscoelastic properties of gelatin-based hydrogels[13,18,19]. These rheological results, while providing independent mechanical characterization of the gelatin matrices, also confirm that the tested formulations differed in their viscoelastic properties. Under current experimental conditions, most notably, the matrices with the highest G' values had lower methylene blue surface spreading and penetration. Although our experiments indicate that increasing stiffness coincides with decreasing dye transport, this should not be taken as proof that this relationship exists independent of other variables. Gelatin concentration likely affects many other factors which could influence dye transport through multiple biological mechanisms, including dye-matrix interactions and structure of the hydrated network; these factors were not able to be studied in isolation[20].

An additional observation was that differences in penetration among gelatin concentrations were relatively small at early time points and became more apparent at later time points. One possible explanation is that surface related processes such as wetting and initial dye-matrix interactions have a higher impact on the early stage of penetration compared to the influence of concentration-dependent matrix that may increase as the dye penetrates deeper in the sample. However, the current experimental setup is not designed to differentiate the individual transport processes. Thus, the time dependence

© The National High School Journal of Science 2026

of the observations does not prove the hypothesis that a shift from surface dominated to network dominated transport occurs over the duration of the experiment.

These results offer a simple experimental system for studying the impact of gelatin concentration on methylene blue spreading and penetration and demonstrate concentration-dependent transport in a three-dimensional gelatin matrix. As shown by the functionally reduced methylene blue spreading and penetration due to concentration changes, these results clearly indicate that variations in gelatin can greatly impact the observed transport dynamics. However, the gelatin concentrations were not matched to specific tumor ECM compositions, mechanical properties, or structural characteristics. Therefore, individual gelatin concentrations should not be interpreted as direct representations of particular normal or tumor tissues due to the fact that these gels represent a simple, well-controlled system to compare methylene blue diffusion under controlled experimental conditions.

In this study, gelatin concentration served as a controlled formulation parameter rather than as a direct measure of specific ECM properties such as stiffness, porosity, pore size, or tortuosity. As noted in the Abstract and Introduction, other ECM properties would need to be characterized independently. In the present study, rheological characterization was performed to assess concentration-dependent viscoelastic properties, whereas hydrated structural properties such as pore size, porosity, tortuosity, and permeability were not directly measured. Instead, this work focuses on the observable relationship between concentration and transport behavior. The methylene blue transport assays - the Droplet Method (surface spread) and Overlay Method (penetration depth) - measure visible dye migration through gelatin matrices. It should be noted that these methods characterize the transport of the dye, including diffusion and capillary flow and possibly other phenomena. The term "dye transport" is used to encompass these phenomena without differentiating diffusion from the other phenomena. In order to determine an effective diffusion coefficient, it requires steady-state transport conditions or a well-defined initial condition and subsequent analysis according to appropriate mass transfer equations; this may be an improvement to the current methods and can be investigated in the future.

The interactions between methylene blue and gelatin should also be considered when interpreting the observed transport behavior[14,15,21]. Methylene blue is a charged dye; therefore, its diffusion behavior may include contributions from dye-gelatin interactions in addition to diffusion in the aqueous phase[14]. Partitioning/adsorption of methylene blue into the gelatin networks was not separately quantified in this study. Other important variables that influence diffusion like ionic strength and pH of the dye solutions were not systematically varied or evaluated as experimental factors. In addition, concentration-dependent optical effects within the gelatin matrices were not independently calibrated. Hence, the observed differences in methylene blue transport cannot be attributed to physical impediments to molecular transport alone. Future studies should include adsorption measurements, partition measurements, optical calibration at the studied concentrations, and good control of the solution conditions to clarify their respective contributions.

The gelatin hydrogel system provides a simplified three-dimensional matrix for examining concentration-dependent transport in a controlled environment[6,7]. However, native tumor ECM is far more complex, composed of collagen, hyaluronic acid, fibronectin, proteoglycans, and numerous biochemical factors[22–24]. Additionally, tumor microenvironments also include interstitial fluid flow, cellular uptake, and enzymatic ECM remodeling, all of which contribute to the complexity of drug delivery and treatment responses in tumors[25]. All of these complexities are not captured by the gelatin system due to its simplicity. Methylene blue is a small, water-soluble model molecule, not an anticancer drug. Actual therapeutics may exhibit different transport patterns due to the fact that they show a high variance in terms of size, hydrophobicity, charge, and binding properties towards the ECM. The findings of this study demonstrate a concentration-dependent transport effect in a simplified gelatin matrix. However, to extend these results to actual drugs or tissues, it will require further investigation using relevant drugs and more sophisticated matrix systems.

Despite these limitations, this study achieves its stated goal of providing a straightforward experimental approach for visualizing how matrix concentration is associated with molecular transport behavior. All experiments have been performed in triplicates with consistent imaging, quantification, and data analysis procedures. Representative time-lapse images have been used to ensure similarity among the images for different concentrations at different times in Figures 1 and 3 whereas Figures 2 and 4 have been constructed by taking mean values with standard deviations of the experiments performed in triplicates. Similarity among the results from replicates supports the reproducibility of the concentration-dependent transport behavior and highlights the reliability of our system for future research. This discussion of transport can be used as a basis for future studies where more realistic biomimetic setups can be implemented. Future studies could include direct measurements of mechanical and structural properties, additional model molecules with different sizes and charges, and therapeutically relevant compounds. They could also focus on developing a quantitative model of transport with specified initial conditions and concentration profiles which match with appropriate mass-transport models. These future studies will be able to highlight whether such simple matrix systems can be used to predict and optimize drug delivery in complex bio-

© The National High School Journal of Science 2026

logical environments.

Conclusion

A simple experimental design for studying concentration-dependent methylene blue transport in three-dimensional gelatin gels was developed in this study. With an increase in gelatin concentration from 1% to 10% (w/v), the extent of methylene blue surface spreading and penetration decreased over the 60 min experiment. Oscillatory rheometry revealed concentration-dependent differences in viscoelastic properties among the matrices, with higher concentrations of gelatin having larger storage moduli (G') under the conditions tested.

SEM imaging also showed that there were concentration-dependent differences in the morphology of freeze-dried gelatin samples. However, because freezing and drying may change the structure of the hydrogel, the results were treated only as a measure of the qualitative morphology of the dried samples rather than pore size, porosity, interconnectivity, tortuosity or permeability of the hydrated gels. Consequently, these results did not demonstrate that variations in hydrated pore architecture or matrix stiffness alone led to the differences observed in the transport of the dye.

Although the mechanisms behind the assays may be complex (as dye spreading and penetration are not necessarily due to diffusion only; these phenomena may result from wetting, capillary flow, and dye-matrix interactions), a relationship between gelatin concentration in a simple matrix and methylene blue transport is reproducibly observed. In addition, the tested gelatin concentrations were not calibrated to specific tumor tissues, and methylene blue was used as a model tracer rather than an anticancer drug. Therefore, although this system can be used as a tool to study concentration-dependent transport in a simplified matrix, it cannot be considered as an exact quantitative model of drug transport in tumor microenvironments.

Further studies that include hydrated-state structural analysis, transport studies with controlled geometries, quantitative modeling of diffusion, and analysis with a number of tracers with different physicochemical properties will be needed in order to understand the reason for concentration-dependent transport and verify that these behaviors would be applicable to biological matrices of higher complexity.

References

1 J. Zhang, W. Han, M. Zhang, Y. Yi, M. Long. Targeting tumor microenvironmental barriers to enhance immunogenic cell death in solid tumors. *Frontiers in Immunology*. Vol. *16*, 2025. https://doi.org/10.3389/fimmu.2025.1672601.

2 P. Gong, F. Wang, Y. Hua, J. Ying, J. Chen, Y. Qiao. Collagenase-mediated extracellular matrix targeting for enhanced drug penetration and therapeutic efficacy in nanoscale delivery systems for cancer therapy. *Journal of Nanobiotechnology*. Vol. *23*, 2025. https://doi.org/10.1186/s12951-025-03815-y.

3 S. Fatima. Tumor Microenvironment: A Complex Landscape of Cancer Development and Drug Resistance. *Cureus*. Vol. *17*, 2025. https://doi.org/10.7759/cureus.82090.

4 X. He, Y. Yang, Y. Han, C. Cao, Z. Zhang, L. Li, C. Xiao, H. Guo, L. Wang, L. Han, Z. Qu, N. Liu, S. Han, F. Xu. Extracellular matrix physical properties govern the diffusion of nanoparticles in tumor microenvironment. *Proceedings of the National Academy of Sciences of the United States of America*. Vol. *120*, 2023, Article e2209260120. https://doi.org/10.1073/pnas.2209260120.

5 S. Ramanujan, A. Pluen, T.D. McKee, E.B. Brown, Y. Boucher, R.K. Jain. Diffusion and convection in collagen gels: implications for transport in the tumor interstitium. *Biophysical Journal*. Vol. *83*, 2002, pp. 1650–1660. https://doi.org/10.1016/S0006-3495(02)73933-7.

6 A.P. Cameron, B. Zeng, Y. Liu, H. Wang, F. Soheilmoghaddam, J. Cooper-White, C.-X. Zhao. Biophysical properties of hydrogels for mimicking tumor extracellular matrix. *Biomaterials Advances*. Vol. *136*, 2022, Article 212782. https://doi.org/10.1016/j.bioadv.2022.212782.

7 O. Degerstedt, P. O'Callaghan, A. L. Clavero, J. Gråsjö, O. Eriksson, E. Sjögren, P. Hansson, F. Heindryckx, J. Kreuger, H. Lennernäs. Quantitative imaging of doxorubicin diffusion and cellular uptake in biomimetic gels with human liver tumor cells. *Drug Delivery and Translational Research*. Vol. *14*, 2024, pp. 970–983. https://doi.org/10.1007/s13346-023-01445-1.

8 E. Dogan, C. Holshue, A. Bhusal, R. Shukla, A.K. Miri. Cell encapsulation in gelatin methacryloyl bioinks impairs microscale diffusion properties. *Frontiers in Bioengineering and Biotechnology*. Vol. *11*, 2023, Article 1193970. https://doi.org/10.3389/fbioe.2023.1193970.

9 A. Talaei, C.D. O'Connell, S. Sayyar, M. Maher, Z. Yue, P.F. Choong, G.G. Wallace. Optimizing the composition of gelatin methacryloyl and hyaluronic acid methacryloyl hydrogels to maximize mechanical and transport properties using response surface methodology. *Journal of Biomedical Materials Research Part B: Applied Biomaterials*. Vol. *111*, 2023, pp. 526–537. https://doi.org/10.1002/jbm.b.35169.

10 T. Gregory, P. Benhal, A. Scutte, D. Quashie J., K. Harrison, C. Cargill, S. Grandison, M.J. Savitsky, S. Ramakrishnan, J. Ali. Rheological characterization of cell-laden alginate-gelatin hydrogels for 3D biofabrication. *Journal of the Mechanical Behavior of Biomedical Materials*. Vol. *136*, 2022, Article 105474. https://doi.org/10.1016/j.jmbbm.2022.105474.

11 S.G. Zambuto, S.S. Kolluru, E. Ferchichi, H.F. Rudewick, D.M. Fodera, K.M. Myers, S.P. Zustiak, M.L. Oyen. Evaluation of gelatin bloom strength on gelatin methacryloyl hydrogel properties. *Journal of the Mechanical Behavior of Biomedical Materials*. Vol. *154*, 2024, Article 106509. https://doi.org/10.1016/j.jmbbm.2024.106509.

12 C.W. Chang, B.L. Dargaville, K.I. Momot, D.W. Hutmacher. An investigation of water status in gelatin methacrylate hydrogels by means of water relaxometry and differential scanning calorimetry. *Journal of Materials Chemistry B*. Vol. *12*, 2024, pp. 6328–6341. https://doi.org/10.1039/d4tb00053f.

13 S. Nogami, K. Kadota, H. Uchiyama, H. Arima-Osonoi, M. Shibayama, Y. Tozuka. Evaluation of the rheological and rupture properties of gelatin-based hydrogels blended with polymers to determine their drug diffusion behavior. *Polymer Journal*. Vol. *54*, 2022, pp. 1477–1487. https://doi.org/10.1038/s41428-022-00681-5.

14 J. Zidek, A. Sudakova, J. Smilek, D.A. Nguyen, H.L. Ngoc, L.M. Ha. Explorative Image Analysis of Methylene Blue Interactions with Gelatin in Polypropylene Nonwoven Fabric Membranes: A Potential Future Tool for the Characterization of the Diffusion Process. *Gels*. Vol. *9*, 2023, Article 888. https://doi.org/10.3390/gels9110888.

15 T. Maeda, S. Tajima, M. Suto, K. Murai. Analysis of Permeation and Re-

© The National High School Journal of Science 2026

lease Behavior Based on Structural Differences in the Gelatin Network within Hydrogels. *Macromolecular Bioscience*. Vol. *25*, 2025, Article e00628. https://doi.org/10.1002/mabi.202400628.

16 C. Morrish, S. Kasapis. Diffusive transport phenomena of lactoferrin from gelatin gels crosslinked with genipin. *Food Hydrocolloids*. Vol. *146*, 2024, Article 109203. https://doi.org/10.1016/j.foodhyd.2023.109203.

17 A. Franco, B. Van Durme, S. Van Vlierberghe, C. Dupont-Gillain. Misleading Pore Size Measurements in Gelatin and Alginate Hydrogels Revealed by Confocal Microscopy. *Tissue Engineering Part C: Methods*. Vol. *30*, 2024, pp. 307–313. https://doi.org/10.1089/ten.tec.2024.0117.

18 H. Yousefi-Mashouf, L. Bailly, L. Orgéas, N. Henrich Bernardoni. Mechanics of gelatin-based hydrogels during finite strain tension, compression and shear. *Frontiers in Bioengineering and Biotechnology*. Vol. *10*, 2023, Article 1094197. https://doi.org/10.3389/fbioe.2022.1094197.

19 S.R. Derkach, N.G. Voron'ko, Y.A. Kuchina, D.S. Kolotova, V.A. Grokhovsky, A.A. Nikiforova, I.A. Sedov, D.A. Faizullin, Y.F. Zuev. Rheological Properties of Fish and Mammalian Gelatin Hydrogels as Bases for Potential Practical Formulations. *Gels*. Vol. *10*, 2024, Article 486. https://doi.org/10.3390/gels10080486.

20 H. B. Aydin, A. Ozcelikkale, A. Acar. Exploiting Matrix Stiffness to Overcome Drug Resistance. *ACS Biomater Sci Eng*. Vol. *10*, 2024. https://doi.org/10.1021/acsbiomaterials.4c00445.

21 A. Straksys, A. Abouhagger, M. Kirsnytė-Šniokė, T. Kavleiskaja, A. Stirke, W.C.M.A. Melo. Development and Characterization of a Gelatin-Based Photoactive Hydrogel for Biomedical Application. *Journal of Functional Biomaterials*. Vol. *16*, 2025, Article 43. https://doi.org/10.3390/jfb16020043.

22 X. Wang, H. Zhang, X. Chen, C. Wu, K. Ding, G. Sun, Y. Luo, D. Xiang. Overcoming tumor microenvironment obstacles: Current approaches for boosting nanodrug delivery. *Acta Biomaterialia*. Vol. *166*, pg. 42-68, 2023. https://doi.org/10.1016/j.actbio.2023.05.043.

23 M. El-Tanani, S. A. Rabbani, R. Babiker, I. Rangraze, S. Kapre, S. S. Palakurthi, A. M. Alnuqaydan, A. A. Aljabali, M. Rizzo, Y. El-Tanani, M. M. Tambuwala. Unraveling the tumor microenvironment: Insights into cancer metastasis and therapeutic strategies. *Cancer Letters*. Vol. *591*, 2024. https://doi.org/10.1016/j.canlet.2024.216894.

24 X. Yi, X. Jin, Y. Hu, Z. Shen, X. Zheng, D. Luo, T. Xu, J. Yan, P. Huang. Drug Delivery Systems for Overcoming Physical Barriers in Cancer Therapy. *Molecular Pharmaceutics*. Vol. *22*, 2025. https://doi.org/10.1021/acs.molpharmaceut.5c00474.

25 M. R. Nikmaneshi, R. K. Jain, L. L. Munn. Computational simulations of tumor growth and treatment response: Benefits of high-frequency, low-dose drug regimens and concurrent vascular normalization. *PLoS Comput Biol*. Vol. *19*, 2023. https://doi.org/10.1371/journal.pcbi.1011131.

© The National High School Journal of Science 2026